

3D π -Conjugated Poly(amic) Acid Polymer as Support Matrices for Ethanol Electro-Oxidation on Palladium and Platinum Catalysts

Victor M. Kariuki¹ · Jing Zhang¹ · Magdalena Parlinska² · Omowunmi A. Sadik¹

Published online: 11 April 2016
© Springer Science+Business Media New York 2016

Abstract The search for new catalyst support matrices to replace the conventional carbon black support has been an important research field for decades. Aromatic conducting polymer (ACP)-based matrices have been found as prospective candidates. Poly(amic) acid (PAA) is one such polymer. We hereby present the catalytic activity and stability of electrodeposited palladium (PdNPs) and platinum (PtNPs) nanoparticles stabilized with PAA. We fabricated four electrodes: Pd/GCE, PAA/Pd/GCE, Pt/GCE, and PAA/Pt/GCE. Cyclic voltammetry and chronoamperometry were employed to assess the ethanol oxidation reaction using PAA as support matrix. PAA was used as support to enhance the stability of PdNPs and PtNPs in basic and acidic media, respectively. The synthesized PAA was characterized using NMR and FTIR. Scanning electron microscopy and X-ray diffraction (XRD) were used for nanoparticle characterization. Test results revealed that the presence of PAA layer on the catalysts leads to sluggish electron transfer kinetics as deduced from higher forward and reverse current densities (5 and 11 mA/cm²) for PdNPs on glassy carbon (Pd/GCE) electrode compared to PAA-stabilized PdNPs (PAA/Pd/GCE) (0.6 and 1.2 mA/cm²), respectively. A similar trend was reported for PtNPs. However, in presence of PAA, both PtNPs and PdNPs were observed to provide stability at up to 900 and 150 cycles, respectively. Chronoamperometric results reinforced the

catalyst stabilization effect of the polymer, with findings revealing that the steady-state current density of PAA/Pd/GCE was ~2.5 times higher than the bare Pd/GCE.

Keywords Palladium nanoparticles · Platinum nanoparticles · Poly(amic) acid · Ethanol oxidation reaction · Electrodeposition · Catalyst stability

Introduction

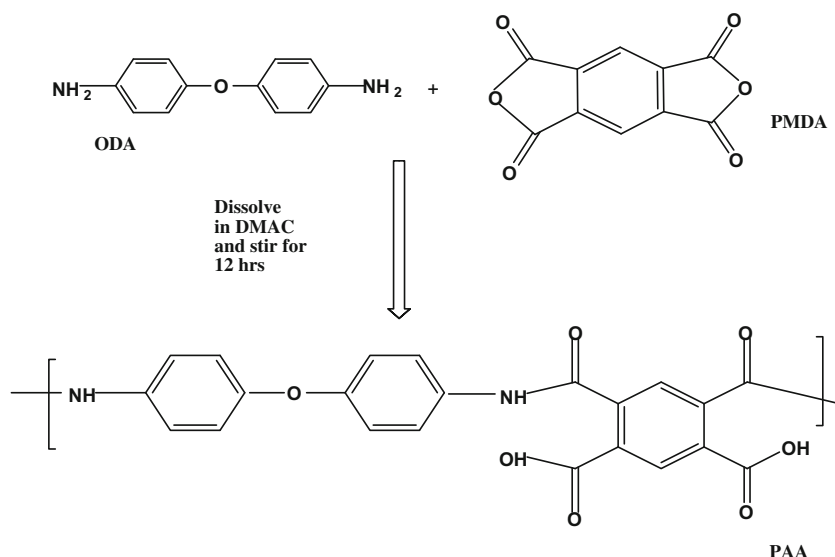
Currently, there is immense interest on fuel cells from both energy and environmental perspectives. Direct alcohol fuel cells (DAFCs) are of great significance as power sources to portable electronic devices [1] due to many advantages accrued to them. DAFCs have high energy density, low operating temperature, ease of handling, and low pollutant emission [2]. Specifically, direct ethanol fuel cells (DEFCs) confer advantages such as high energy density excellent stability and easy storage [3]. Most importantly, ethanol is a renewable resource that can be obtained from agricultural feedstocks such as cereals and maize via fermentation [4–7] and is less toxic compared to methanol. Similarly, nanomaterials play a significant role as a catalyst to oxidize organic matter and convert chemical energy into electricity with high energy density, high energy conversion efficiency, low operating temperature, and environmental friendliness, which are suitable for DEFCs [8]. However, low efficiency of ethanol oxidation has posed a major challenge to the commercialization of DEFCs [9].

Platinum-based catalysts have extensively been proven to be excellent electrocatalysts for electro-oxidation of methanol and ethanol [10–13]. Platinum model catalysts are well known as highly active catalysts for oxidation of small alcohols, including ethanol in acidic media [14]. However, the scarcity of

✉ Omowunmi A. Sadik
OSADIK@BINGHAMTON.EDU

¹ Department of Chemistry, Center for Advanced Sensors and Environmental Systems (CASE), State University of New York at Binghamton, P.O. Box 6000, Binghamton, NY 13902, USA

² Facility for Electron Microscopy and Sample Preparation, University of Rzeszow, Rzeszow, Poland

Scheme 1 Formation of PAA

platinum on the earth makes it expensive for commercialization as a catalyst. Palladium stands out as an effective anode catalyst over platinum because of two main reasons: First, extensive literature shows that Pd exhibits higher catalytic activity and is more stable for ethanol and methanol oxidation in alkaline medium [15]. Secondly, Pd is at least 50 times more abundant on the earth than Pt and therefore less expensive [16].

Previously, conductive substrates (e.g., carbon-based) have been selected as supports to disperse nanoparticle catalysts. For example, highly dispersed palladium nanoparticles on carbon nanotubes (CNTs), carbon fibers Vulcan XC-72 (VXC), etc. exhibit enhanced electrocatalytic activities toward ethanol electro-oxidation [17, 18]. However, the carbon-containing cathode catalyst is subjected to slow and continuous corrosion. Exploitation of new catalyst supporting matrices, to replace the conventionally used carbon black support, has been an important research field for the last couple of years [19–24]. The use of aromatic conducting polymer (ACP)-based matrices as supporting materials for catalyst is emerging as viable alternative [25, 26]. Several conducting polymers (such as polyaniline, polythiophene, PEDOT, and

polypyrrole) are currently being investigated as support matrices. ACPs are being considered on account of their high electroactivity, good reversibility, chemical stability for various electrochemical reactions, as well as the possibility of incorporating noble metal catalysts for the electro-oxidation of small molecules such as hydrogen, methanol and formic acid et cetera [27–31].

Synergistic effect between the metal and the polymer matrices has been reported to provide electrocatalytic performance of the metal/polymer composites in terms of their activity as well as stability [32, 33]. Among the π -conjugated polymers, *poly(amic acid) (PAA)* is an interesting research target due to its fascinating physicochemical properties. PAA exhibits good mechanical strength [34, 35], chemical stability [34], electronic conductivity [36], and facile synthetic route [37, 38]. PAA is also predicted to provide enhanced synergistic interaction with the catalyst particles due to the presence of heteroatoms that make it promising for applications in electrochemical [39] and bioelectrochemical sensors [40, 41]. Consequently, PAA can serve as a unique catalyst support.

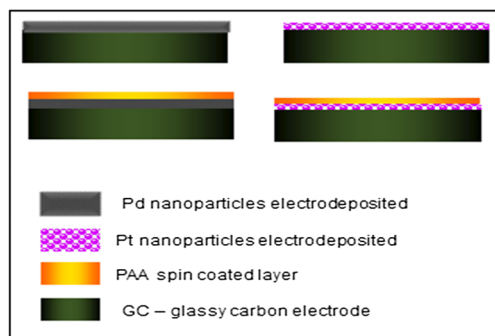
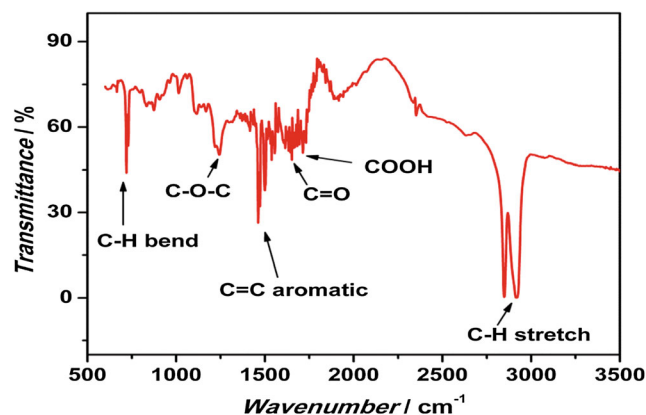
**Fig. 1** Schematic depiction of the four electrodes used in this study**Fig. 2** FTIR spectra of PAA

Table 1 Vibrational assignment for PAA

Bond	Frequency range/cm ⁻¹
C–H	1000–675(s) bend
C–O–C	1225 stretching vibration of ether group
COOH	2610 broad, 1716 stretch
C=C	1450 (aromatic ring C=C str)
C=O	1660 (w) stretch. amide
N–H	3500–3300(m) stretch. amide
C–H	2890, 3000 (SP ² C–H str)

We hypothesize that introducing PAA onto the electrode catalyst layer renders the use of Pd/Pt more effective by enhancing stability of nanoparticles into the electroactive solution.

In this work, we report, for the first time, the use of conductive π -conjugated poly(amic) acid as a support for Pd and Pt nanoparticles in ethanol oxidation reaction in acidic and basic media. We also demonstrate the electrodeposition of Pd and Pt nanoparticles from their precursor salts onto a 3-mm glassy carbon electrode by cycling voltage. The electrodeposited Pd/Pt nanoparticles were spin coated using 0.21 M

poly(amic) acid and was employed for ethanol oxidation reaction. Subsequently, we determined the electrochemical properties of the PAA-supported catalyst systems and finally analyzed the prospects of using PAA as catalyst support for DMFCs.

Experiment

Chemicals used in this study were of analytical grades unless otherwise stated: HCl, HClO₄, PdCl₂, NaOH, PtCl₄, ethanol (EtOH), N,N-dimethylformamide(DMF), N,N-dimethylacetamide (DMAC), 4'-oxidianiline (ODA), and pyromellitic dianhydride (PMDA) were obtained from Sigma-Aldrich (St Louis MO) and used without further purification. Major characterization instruments employed include a scanning electron microscope, AUTOLAB potentiostat-PGSTAT204, BRUKER 600 MHz NMR operated by Topspin™ 3.0 NMR software XRD diffractometer, Spin coater (CHEMAT Technology-KW-4A) and Digimatic micrometer (MDH-25 M-Mitutoyo Corporation)

Poly(amic) acid (0.21 M) used was synthesized as follows: In a vial, 210.25 mg of ODA was added followed by 3.5 to

Fig. 3 a ¹H NMR and b ¹³C NMR spectra of PAA

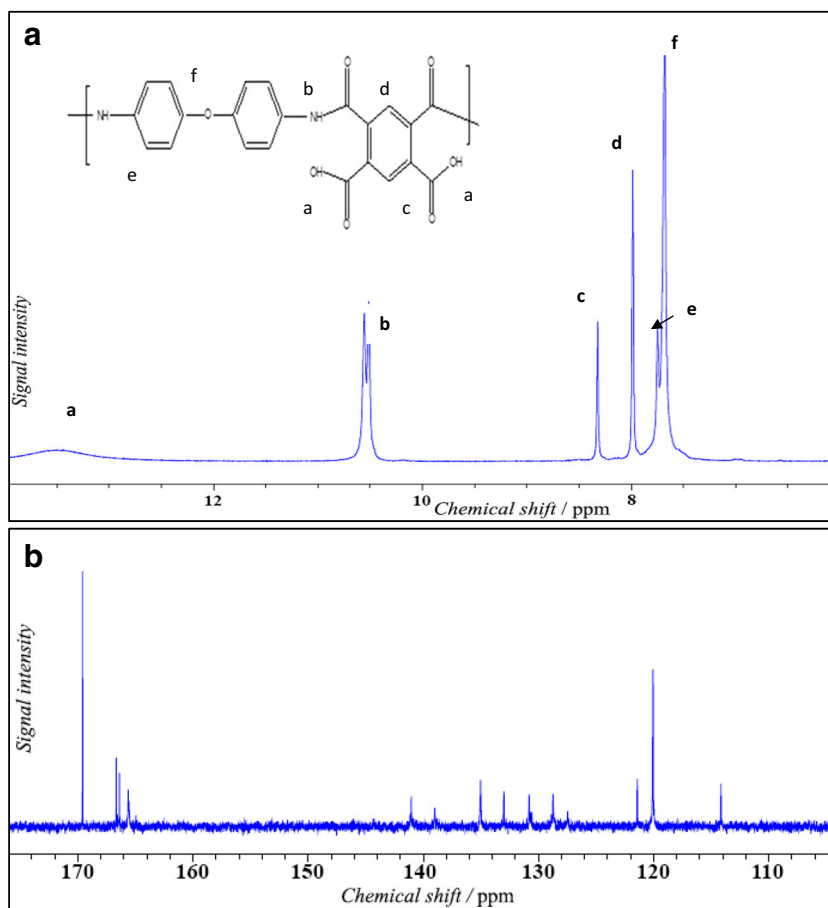
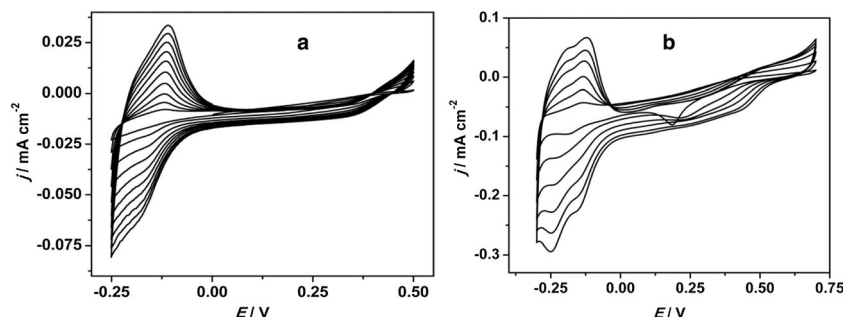


Fig. 4 CV profiles for the electrodeposition of PdNPs (a) (10 scans at 25 mV/s) and PtNPs (b) (6 scans at 25 mV/s)



4 mL of DMF dispensed into the vial using a syringe and then was stirred until complete dissolution of ODA was observed. This was followed by the addition of 229.02 mg PMDA and 1 mL of DMAC into the vial. The vial was then covered with either a box container or aluminum foil after capping and then stirred for 12 h at room temperature. The formation and structure of PAA is shown in Scheme 1.

Electrodeposition of Catalysts and Ethanol Oxidation Reaction

The glassy carbon electrode (GCE; BASi, West Lafayette, IN) was pretreated using the following process: First, the surface of a GCE was polished with 1.0 and 0.5- μm α -alumina powders in sequence, rinsed thoroughly twice with distilled water and placed in a water-filled ultrasonic bath over a 2-min period.

A conventional three electrode electrochemical cell was used for electrodeposition studies. A carbon mesh of large surface area was used as the counter electrode, Ag/AgCl as the reference electrode (BASi, West Lafayette, IN) and the 3.0-mm GCE as working electrode. The cell was cleaned thoroughly before each experiment and kept in a hot oven at 70 °C for at least 1 h before the start of the experiment.

After GCE was dried in air, Pd nanoparticles was grown on the GCE by electrodeposition in a solution containing 2.0×10^{-4} M PdCl₂ and 0.01 M HCl at a potential window of -0.25 to 0.5 V (vs Ag/AgCl)—the resulting Pd nanoparticles supported by GCE is denoted as (Pd/GCE). After the electrodeposition, the modified electrodes were rinsed twice in water and air-dried at room temperature for characterization and further use. Similarly Pt nanoparticles were electrodeposited on GCE in a solution containing 8×10^{-4} M PtCl₄ in 0.01 M HCl. The solution was stirred and purged for 10 min with nitrogen gas before deposition. Potential was cycled between -0.25 and 0.7 V for several scans to achieve a layer of PtNPs on the surface of GCE (denoted as Pt/GCE)

To support the nanoparticles (Pd and Pt) on the electrode surface, 200 μl of poly(amic) acid was dropped on the electrode surface, spin coated at 300 rev/min, and dried for 16 h and then used for further analysis. Under these conditions, an ~ 4 - μm thick film was formed on the electrode surface. The

resultant electrodes are denoted as PAA/Pd/GCE and PAA/Pt/GCE, respectively, as shown in Fig. 1. EOR on PdNPs was conducted in basic media using 1 M NaOH and 1 M EtOH on PdNPs/GCE and PAA/PdNPs/GCE. On the other hand EOR on PtNPs was conducted in acidic media using different concentration of HClO₄ and EtOH.

Surface and Morphological Characterization

Scanning electron microscopy and EDS analyses were performed using a Zeiss Supra 55 VP analytical ultrahigh resolution FESEM+EDAX Pegasus EDS+EBSD equipped with SmartSEM™. The accelerating voltage for SEM was 5 kV whereas that for EDX was 10 kV. All electroanalytical analyses were performed on an autolab potentiostat (model AUT83356) fitted with the Nov. 1.10 software for analyses. Spin coating was conducted on CHEMAT TECHNOLOGY spin coater (KW-4A). The film thickness was measured using Digimatic micrometer (Mitutoyo Corporation)

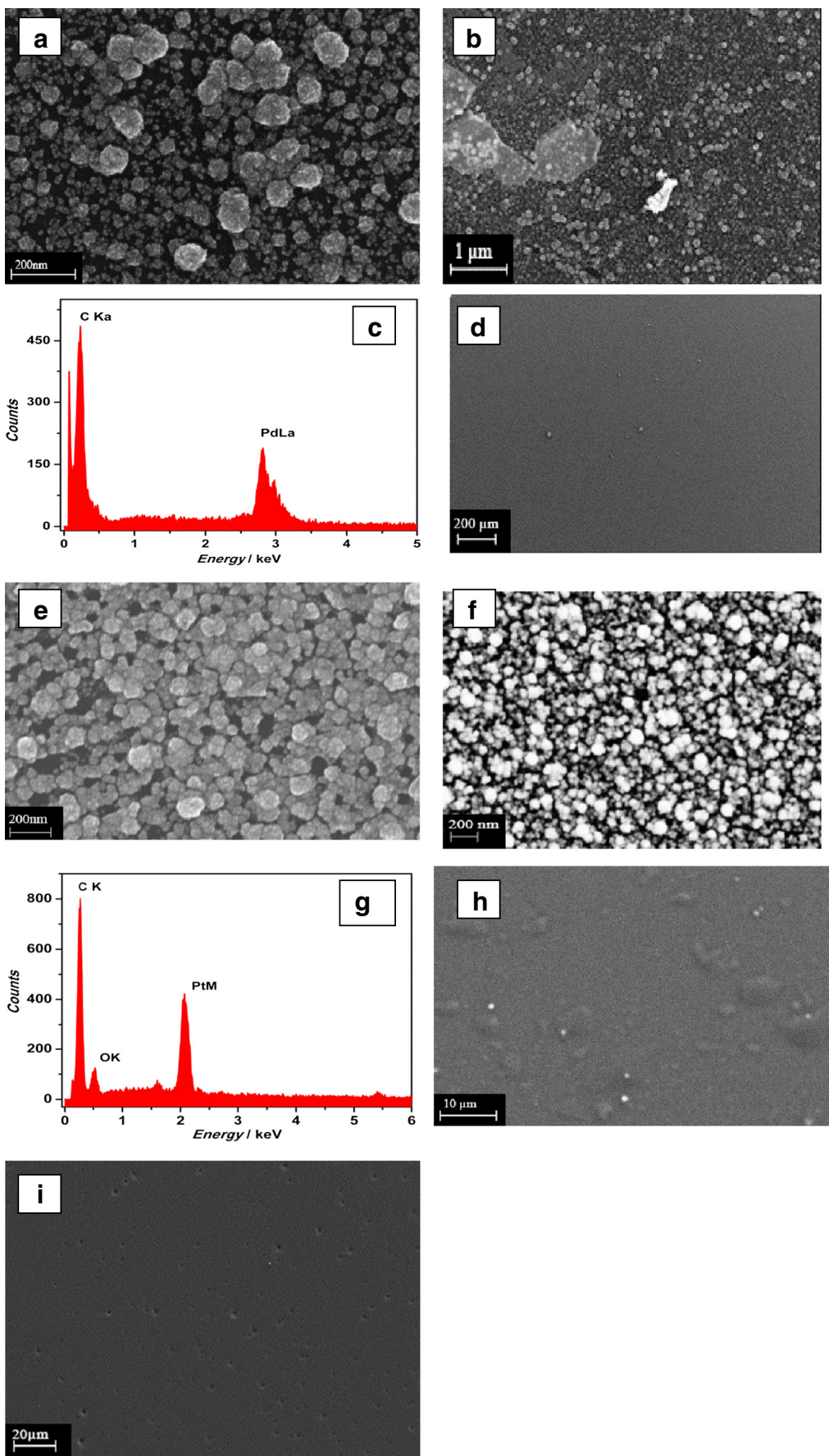
Results and Discussion

NMR and FTIR Characterization of PAA

Typical FTIR spectrum of PAA is shown in Fig. 2. The PAA spectrum exhibited a broad shoulder at 2610 and 1716 cm^{-1} stretch attributed to the COOH bond. The peaks appearing at frequencies of 1225, 1450, and 1660 cm^{-1} could be attributed to the stretching vibration of ether group (C–O–C), C=C (aromatic ring), and C=O bond, respectively. The peaks appearing between 3500 and 3300 cm^{-1} are due to N–H secondary amide stretch. Peaks at 2890 and 3000 cm^{-1} are as a result of the sp² C–H stretching of polymer. The C–H bond bending frequency range is 1000–675 cm^{-1} . The wave numbers for each functional group are summarized in Table 1

The ¹H-NMR (Fig. 3a) of the synthesized PAA was recorded in the range of 5 to 15 ppm. The peaks appearing between

Fig. 5 SEM micrographs of Pd (a, b) and Pt (e, f) showing electrodeposited nanoparticles, EDX spectra of Pd (c) and Pt (g) and SEM images after spin coating PdNPs (d) and PtNPs (h) with PAA. i Bare glassy carbon surface



10 and 11 ppm were attributed to the presence of amide groups in PAA. The peaks occurring at 6.5 and 9 ppm were assigned to the aromatic protons. The soft broad peak around 13.5 ppm was attributed to the carboxylic protons present. In the case of ^{13}C -NMR (Fig. 3b), the solvent peak (DMSO- D_6) appeared at around 39 ppm, as is expected (not shown). The peaks appearing between ~ 115 and ~ 142 ppm were assigned to the aromatic carbons. The anhydride and amide groups present in the polymers were assigned to the two peaks appearing between ~ 164 and ~ 167 ppm. The peak at 169 ppm is assigned to the DMAC carbon used as a solvent in PAA preparation.

Electrodeposition, Morphological and Electrochemical Characterization of Nanoparticles

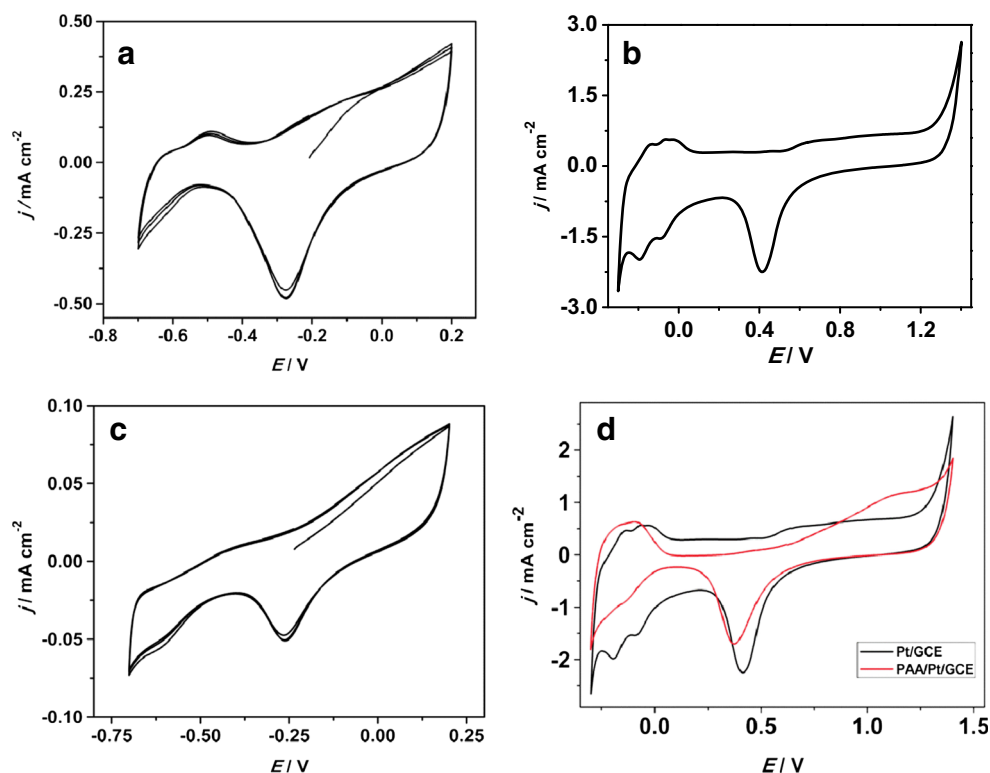
Figure 4 shows the CV profiles for the electrodeposition of PdNPs and PtNPs on the electrode surface. In both cases, the electrodeposition took place at a potential of ~ -0.2 V. The voltammograms obtained are typical of Pd [42, 43] and Pt, respectively.

Figure 5 shows the typical SEM images of as-prepared Pd and Pt structures, indicating that the GCE substrate is covered by almost spherical Pd/Pt structures with diameters in the range of 5–100 nm. A local view of one Pd sphere further revealed that the Pd structure consists of small nanoparticles. The similar observation was recorded for Pt nanoparticles. However, some uncoated GC surface could be seen with some small Pd/Pt islands. The size of small particles was in the

range of 5–20 nm and the larger agglomerates were up to 100 nm in diameter. EDX confirmed the presence of Pd and Pt nanoparticles on the electrode surface (Fig. 5c, g). On spin coating with PAA, the nanoparticles were no longer visible on the surface of the GCE (Fig. 5d, h). The appearance of bare glassy carbon electrode is shown in Fig. 5

Before the ethanol oxidation measurements, the electrodeposited Pd and Pt electrodes were subjected to potential cycling in deaerated solution (1 M NaOH and 0.1 M HClO_4 , respectively) in order to clean and electrochemically characterize the Pd and Pt surface. The cyclic voltammograms presented in Fig. 6 show the general features characteristic to palladium and platinum electrodes. Palladium and platinum redox processes are pH dependent [42, 44, 45]. According to the literature, for a potential range above -150 mV, there was a formation of palladium [31] oxide layer on the surface of the catalyst [46]. The broad anodic peak at the potentials (-0.4 to -0.2 V) is associated with the formation of Pd surface oxides under basic conditions, and the reduction of these oxides gives a well-defined cathodic peak between -0.4 and -0.2 V (Fig. 6a) while Pt oxides form around 0.4 V under acidic conditions [44]. The current increase between 0.0 V and -0.2 V (Fig. 6b) is attributed to hydrogen adsorption and desorption [42, 45]. The charge corresponding to the Pd and Pt oxide reduction peak was used to determine the real electroactive surface area.

Fig. 6 Cyclic voltammograms for Pd/GCE, Pt/GCE, PAA/Pd/GCE, and PAA/Pt/GCE electrodes in nitrogen-saturated solutions **a** Pd/GCE—1 M NaOH, **b** Pt/GCE—0.1 M HClO_4 , **c** PAA/Pd/GCE—1 M NaOH, and **d** PAA/Pt/GCE and Pt/GCE; scan rate 50 mV s^{-1}



In the presence of PAA (Fig. 6c, d), the redox peaks in both Pd and Pt reduced probably due to the sluggish accessibility to the electroactive surface. The π -conjugated polymer could shuttle electrons, and owing to its conductive nature, the electroactivity of the catalysts is retained. Also, as indicated in subsequent data, the presence of the polymer ensures that the nanoparticles remain intact on the electrode surface without peeling off into solution.

EOR on Pd/GC and PAA/Pd/GC Electrodes in Alkaline Media

Figure 7a shows the voltammogram obtained in 1 M NaOH/1 M EtOH with a glassy carbon electrode

modified by electrodeposited PdNPs on its surface as depicted. The voltammograms are typical of EOR in alkaline media on Pd catalysts [47–49]. The effectiveness of the catalyst support used in this work was determined using the output peak current densities. PdNPs supported on PAA exhibited a lower forward peak current density (0.6 mA/cm^2) compared to electrodeposited PdNPs without polymer support (5 mA/cm^2) (Fig. 7a, c respectively).

The onset potential was another feature that we deduced from the voltammogram. PdNPs without polymer support has an onset potential of -600 mV compared to -400 mV of PAA-supported PdNPs. PdNPs has also a higher backward current peak maxima (11 mA/cm^2)

Fig. 7 EOR on Pd/GCE (a) and PAA/Pd/GCE (first scan) (c) at 50 mV/s and stability studies (100 scans) at 100 mV/s of Pd/GCE (b) and PAA/Pd/GCE (d). e Chronoamperograms of Pd/GCE and PAA/Pd/GCE in 1 M EtOH and 1 M NaOH at room temperature; applied potential is -0.2 V

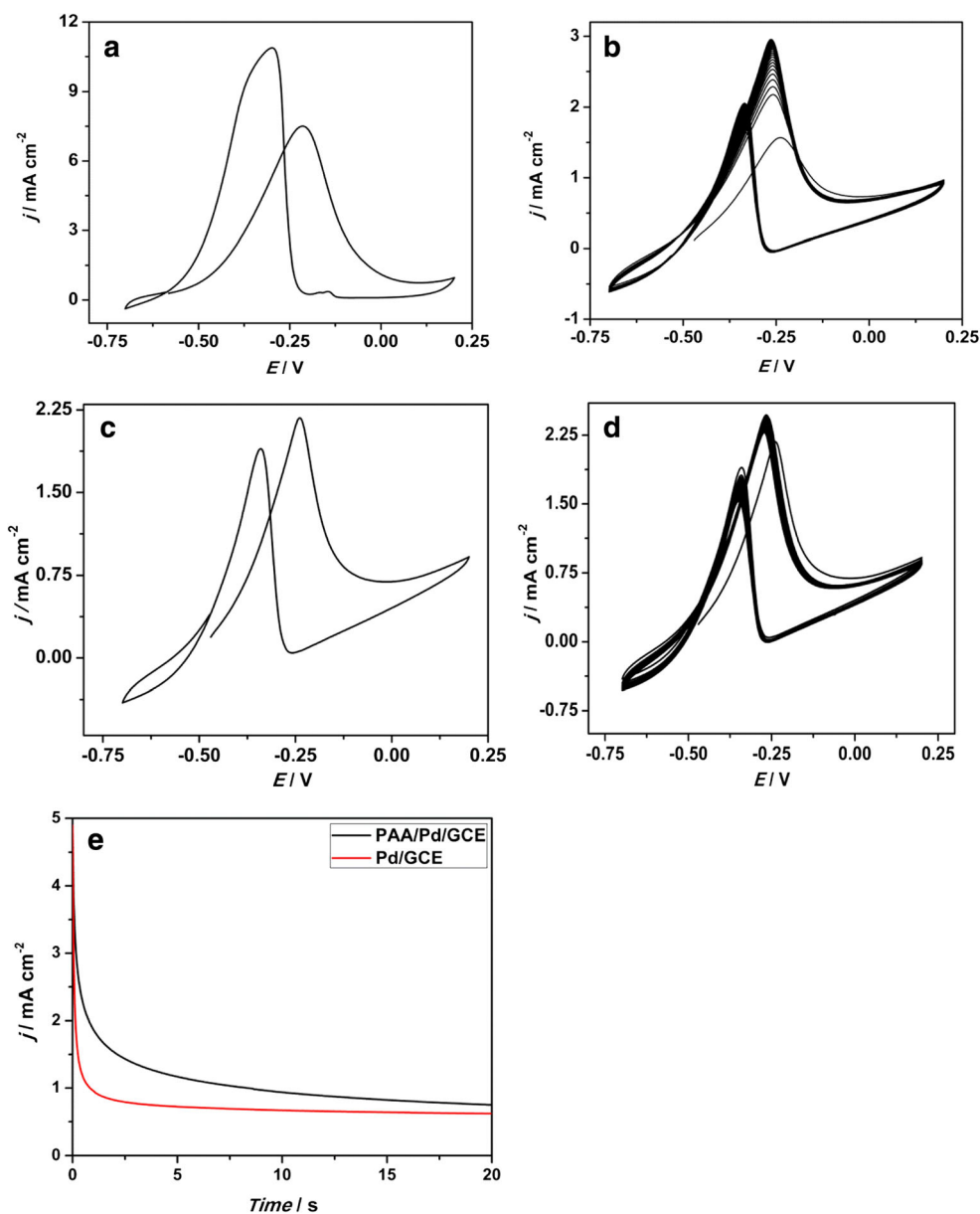
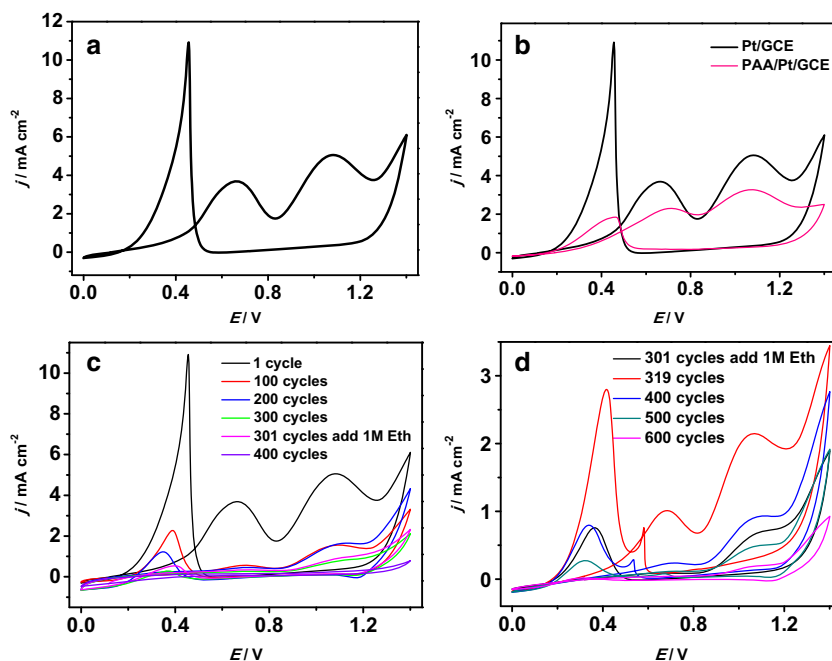


Fig. 8 **a** CV of ethanol oxidation reaction (EOR) in 0.1 M HClO₄ and 1 M EtOH on Pt/GCE; **b** superimposed CV of EOR in 0.1 M HClO₄ and 1 M ethanol on Pt/GCE and PAA/Pt/GCE; **c** CV of EOR in 0.1 M HClO₄ and 1 M EtOH showing decline of current after 400 scans; **d** stability study of PAA/Pt/GCE



compared to 1.2 mA/cm² for PAA-supported PdNPs. These results point to a drag in the kinetics of ethanol oxidation in the presence of PAA support. However, besides these, the catalysts showed great stability with little decrease in peak current densities after 100 scans in the presence of PAA support (Fig. 7d). The decreased kinetics was as a result of the time taken by ethanol to diffuse across the porous PAA layer to the PdNPs and also the semiconducting nature of PAA. Figure 7e shows the chronoamperograms (current-time transients) recorded for the oxidation of ethanol (1 M) on the Pd/GCE and PAA/Pd/GCE in basic media at potential of -0.2 V. Both electrodes presented continuous slight decay in activity during the time of study. As shown, the current density of the Pd/GCE catalyst behaved with a steeper decreasing trend which was possibly due to the instability of Pd on GCE. The steady-state current density of PAA/Pd/GCE is almost 2.5 times higher than the Pd/GCE reaffirming the stabilizing effect of PAA on the catalyst.

EOR on Pt/GCE and PAA/Pt/GCE Electrodes in Acidic Media

Figure 8 shows the typical voltammograms of the EOR on Pt/GCE in acidic media [14, 50]. Pt/GCE (Fig. 8a) exhibits higher current densities which decline on the PAA/Pt/GCE (Fig. 8b) due to sluggish electron transfer kinetics occasioned by the layer of polymer on the Pt catalysts. However, in the presence of the polymer

layer, the Pt catalyst was more stable (Fig. 8d). PAA/Pt/GCE remained stable at up to 900 cycles (result not shown), unlike Pt/GCE whose current flattened out barely after 300 cycles (Fig. 8c).

Conclusion

In this study, PtNPs and PdNPs were electrodeposited on GCE. PAA was spin-coated over the electrodeposited catalysts and explored as a possible catalyst support. PAA, a novel π -conjugated polymer, was explored as a catalyst support due to its mechanical strength, porosity, electron conductivity, and stability in acidic and basic media. Despite reduction in current density in presence of PAA layer on the catalyst, the catalytic activity of the PtNP/PdNP catalysts is retained. Moreover, there is enhanced catalyst stability in presence of the polymer layer. This study therefore demonstrates the stability of PAA/Pt/GCE and PAA/Pd/GCE over Pt/GCE and Pd/GCE electrocatalysts for EOR in acidic and alkaline media, respectively. Despite the sluggish electron kinetics, these results present new possibilities in exploiting PAA as a possible alternative ACPs as effective catalyst support matrix for the oxidation of ethanol in DMFCs.

Acknowledgments The authors acknowledge the National Science Foundation (DMR 1007900) for funding.

References

1. J. Bangyang, H. Tang, M. Pan, *Int. J. Hydrog. Energy* **37**, 4612 (2012)
2. J. Yang, Y. Xie, R. Wang, B. Jiang, C. Tian, G. Mu, J. Yin, B. Wang, H. Fu, *ACS Appl. Mater. Interfaces* **5**, 6571 (2013)
3. W. Zhou, S.Q. Song, W.Z. Li, Z.H. Zhou, G. Sun, Q. Xin, S. Douvartzides, P. Tsiakaras, *J. Power Sources* **140**, 50 (2005)
4. L.R. Lynd, C.H. de Brito Cruz, *Science (Washington)* **330**, 1176 (2010)
5. E.A. Davidson, *Science* **330**, 1176 (2010)
6. S.C. Lai, M.T. Koper, *Phys. Chem. Chem. Phys.* **11**, 10446 (2009)
7. D. Yuan, X. Yuan, W. Zou, F. Zeng, X. Huang, S. Zhou, *J. Mater. Chem.* **22**, 17820 (2012)
8. S. Ghosh, A.-L. Teillout, D. Floresyona, P. de Oliveira, A. Hagege, H. Remita, *Int. J. Hydrog. Energy* **40**, 4951 (2015)
9. F. Vigier, S. Rousseau, C. Coutanceau, J.-M. Leger, C. Lamy, *Top. Catal.* **40**, 111 (2006)
10. L. Dong, R.R.S. Gari, Z. Li, M.M. Craig, S. Hou, *Carbon* **48**, 781 (2010)
11. R.-S. Juang, C.-T. Hsieh, J.-Q. Hsiao, H.-T. Hsiao, D.-Y. Tzou, M.M. Huq, *J. Power Sources* **275**, 845 (2015)
12. L. Wang, M. Bevilacqua, J. Filippi, P. Fornasiero, M. Innocenti, A. Lavacchi, A. Marchionni, H. Miller, F. Vizza, *Appl. Catal. B Environ.* **165**, 185 (2015)
13. J.M. Jacob, P.G. Corradini, E. Antolini, N.A. Santos, J. Perez, *Appl. Catal. B Environ.* **165**, 176 (2015)
14. R.B. Kutz, B. Braunschweig, P. Mukherjee, R.L. Behrens, D.D. Dlott, A. Wieckowski, *J. Catal.* **278**, 181 (2011)
15. K.-H. Ye, S.-A. Zhou, X.-C. Zhu, C.-W. Xu, P.K. Shen, *Electrochim. Acta* **90**, 108 (2013)
16. A.Y. Tsivadze, M. Tarasevich, V. Andreev, V. Bogdanovskaya, *Russ. J. Gen. Chem.* **77**, 783 (2007)
17. J. Zhang, Y. Mo, M. Vukmirovic, R. Klie, K. Sasaki, R. Adzic, *J. Phys. Chem. B* **108**, 10955 (2004)
18. F. Ksar, G. Surendran, L. Ramos, B. Keita, L. Nadjjo, E. Prouzet, P. Beaunier, A. Hagege, F. Audonnet, H. Remita, *Chem. Mater.* **21**, 1612 (2009)
19. Y.-J. Wang, D.P. Wilkinson, J. Zhang, *Chem. Rev.* **111**, 7625 (2011)
20. S. Sharma, B.G. Pollet, *J. Power Sources* **208**, 96 (2012)
21. S. Biallozor, A. Kupniewska, V. Jasulaitene, *Fuel Cells* **3**, 8 (2003)
22. Z. Chen, L. Xu, W. Li, M. Waje, Y. Yan, *Nanotechnology* **17**, 5254 (2006)
23. S. Patra, N. Munichandraiah, *Langmuir* **25**, 1732 (2008)
24. M. Zhiani, B. Rezaei, J. Jalili, *Int. J. Hydrog. Energy* **35**, 9298 (2010)
25. K. Dutta, S. Das, D. Rana, P.P. Kundu, *Polym. Rev.* **55**, 1 (2015)
26. K. Dutta, S. Das, P.P. Kundu, *J. Membr. Sci.* **468**, 42 (2014)
27. T. Maiyalagan, *J. Power Sources* **179**, 443 (2008)
28. B. Vercelli, G. Zotti, A. Berlin, *J. Phys. Chem. C* **113**, 3525 (2009)
29. P. Xu, X. Han, B. Zhang, Y. Du, H.-L. Wang, *Chem. Soc. Rev.* **43**, 1349 (2014)
30. W.M. Millán, T.T. Thompson, L. Arriaga, M.A. Smit, *Int. J. Hydrog. Energy* **34**, 694 (2009)
31. F.-J. Liu, L.-M. Huang, T.-C. Wen, A. Gopalan, *Synth. Met.* **157**, 651 (2007)
32. M.H. Seo, E.J. Lim, S.M. Choi, H.J. Kim, W.B. Kim, *Top. Catal.* **53**, 678 (2010)
33. M.H. Seo, E.J. Lim, S.M. Choi, S.H. Nam, H.J. Kim, W.B. Kim, *Int. J. Hydrog. Energy* **36**, 11545 (2011)
34. N. Du, C. Wong, M. Feurstein, O.A. Sadik, C. Umbach, B. Sammakia, *Langmuir* **26**, 14194 (2010)
35. I. Yazgan, N. Du, R. Congdon, V. Okello, O.A. Sadik, *J. Membr. Sci.* **472**, 261 (2014)
36. O. Sadik, N. Du, V. Kariuki, V. Okello, V. Bushlyar, *ACS Sustainable Chem. Eng.* **2**, 1707 (2014)
37. M.A. Omole, V.A. Okello, V. Lee, L. Zhou, O.A. Sadik, C. Umbach, B. Sammakia, *ACS Catal.* **1**, 139 (2011)
38. V.M. Kariuki, I. Yazgan, A. Akgul, A. Kowal, M. Parlinska, O.A. Sadik, *Environ. Sci.: Nano* **2**, 518 (2015)
39. V. M. Kariuki, S. A. Fasih-Ahmad, F. J. Osonga and O. A. Sadik, *Analyst* (2016)
40. N.M. Noah, M. Omole, S. Stern, S. Zhang, O.A. Sadik, E.H. Hess, J. Martinovic, P.G. Baker, E.I. Iwuoha, *Anal. Biochem.* **428**, 54 (2012)
41. O.A. Sadik, S.K. Mwilu, A. Aluoch, *Electrochim. Acta* **55**, 4287 (2010)
42. V.C. Diculescu, A.-M. Chiorcea-Paquim, O. Corduneanu, A.M. Oliveira-Brett, *J. Solid State Electrochem.* **11**, 887 (2007)
43. M.I. Prodromidis, E.M. Zahran, A.G. Tzakos, L.G. Bachas, *Int. J. Hydrog. Energy* **40**, 6745 (2015)
44. G. Chang, Y. Luo, W. Lu, X. Qin, A.M. Asiri, A.O. Al-Youbi, X. Sun, *Am. J. Nanotechnol.* **4**, 1 (2013)
45. M. Grdeń, M. Łukaszewski, G. Jerkiewicz, A. Czerwiński, *Electrochim. Acta* **53**, 7583 (2008)
46. J. Prabhuram, R. Manoharan, H. Vasan, *J. Appl. Electrochem.* **28**, 935 (1998)
47. Z. Liang, T. Zhao, J. Xu, L. Zhu, *Electrochim. Acta* **54**, 2203 (2009)
48. C. Bianchini, P.K. Shen, *Chem. Rev.* **109**, 4183 (2009)
49. N. Li, Y.-X. Zeng, S. Chen, C.-W. Xu, P.-K. Shen, *Int. J. Hydrog. Energy* **39**, 16015 (2014)
50. J.F. Gomes, K. Bergamaski, M.F. Pinto, P.B. Miranda, *J. Catal.* **302**, 67 (2013)